https://doi.org/10.32604/zkg.2026.078108

ARTICLE

# Feasibility study of applying petrochemical-derived gypsum from the petrochemical industry in controlled low strength materials

**Jie Chen[1], An Cheng[1], Kinga Korniejenko[2] and Wei-Ting Lin[1,*]**
[1]Department of Civil Engineering, National Ilan University, Ilan, Taiwan
[2]Faculty of Materials Engineering and Physics, Cracow University of Technology, Kraków, Poland
*Corresponding Author: Wei-Ting Lin. Email: wtlin@niu.edu.tw

Received: 24 December 2025; Accepted: 02 April 2026

ABSTRACT: The massive accumulation of petrochemical-derived gypsum (PDG) poses significant environmental management challenges, necessitating innovative valorization strategies within the circular economy. This study investigated the engineering feasibility and ecological safety of repurposing gypsum as a functional aggregate substitute in the production of controlled low-strength materials, aiming to reduce reliance on natural resources while effectively managing industrial waste. The experimental program was conducted in two distinct stages using a binder system of Type I Portland cement and Class F fly ash. Stage I evaluated the potential of maximum waste diversion by completely replacing natural fine aggregates with gypsum (100% replacement). Stage II focused on optimizing the mix for industrial viability by reducing the gypsum content to 50% and 37%, thereby partially reintroducing natural coarse and fine aggregates to improve volumetric stability. The study assessed mechanical properties through compressive strength testing under air-curing and water-curing regimes. It evaluated environmental impact via seawater immersion tests, pH monitoring, and toxicity characteristic leaching procedures. The investigation revealed that the 100% PDG mixture achieved a 28-day compressive strength of 4.69 MPa due to an ettringite-driven air-hardening mechanism but exhibited moisture sensitivity. Conversely, the 37% PDG substitution yielded the highest strength (4.72 MPa) with superior volumetric stability. Leaching assessments confirmed that heavy metal concentrations and pH remained within regulatory limits. Consequently, the 37% replacement ratio provided the optimal balance between mechanical performance and durability, validating the feasibility of materials for sustainable coastal infrastructure and road sub-base applications.

KEYWORDS: Circular economy; ettringite; leaching behavior; sustainable infrastructure

## 1 Introduction

The cement and concrete industry has historically constituted approximately 7 to 8% of global $CO_2$ emissions, rendering the 2050 net-zero target a complex challenge that requires multifaceted strategic interventions [1, 2]. Research emphasized the reduction of the clinker factor as a pivotal measure, given the high carbon intensity of the clinkering process [3, 4]. To this end, supplementary cementitious materials, including fly ash, limestone, and calcined clay, were used to partially replace Portland cement [5]. This practice simultaneously mitigates emissions by 6% to 70% and addresses solid waste management [6]. Additionally, alternative binders, such as geopolymer cement and alkali-activated materials, were investigated for their potential to decarbonize. However, studies acknowledged that specific alternatives, particularly alkali-activated materials (AAMs), entailed production complexities and elevated costs [3, 6, 7].

Controlled low-strength material (CLSM) was characterized as a self-leveling and self-compacting cementitious alternative to conventional structural backfill, distinguished by its capacity to incorporate a diverse array of industrial by-products and waste materials [8]. This approach was identified as a key strategy for mitigating greenhouse gas emissions associated with the production of ordinary Portland cement while simultaneously addressing industrial waste accumulation issues [9]. Research has demonstrated the successful utilization of various waste streams, ranging from mineral admixtures such as fly ash and slag to recycled aggregates and municipal incineration ash, within CLSM formulations [10–12]. Consequently, the integration of these materials was recognized as a well-established green application that aligned civil infrastructure development with circular economy objectives and sustainable engineering practices.

Investigations into the use of recycled gypsum powder as a partial cement substitute in CLSM and

MATERIALS

concrete revealed a complex trade-off between sustainability and mechanical performance [13]. While the singular incorporation of waste gypsum typically resulted in reduced compressive strength and increased water demand, studies demonstrated significant synergistic effects when combined with supplementary cementitious materials (SCMs) such as fly ash. Specifically, optimized mixtures, such as those replacing cement with 20% gypsum and 50% fly ash, exhibited enhanced long-term strength and durability, even in aggressive environments, despite observations of increased moisture absorption and volumetric expansion [13]. Although wide-scale infrastructure adoption was historically constrained by low early-age strength and water sensitivity [14, 15], these composite materials were recognized for their potential in road base applications and their substantial contribution to eco-efficiency through waste diversion and reduced carbon footprints [16].

Natural and industrial by-product gypsums, such as phosphogypsum and flue gas desulphurization gypsum (FDG), were utilized in cement manufacturing to address resource limitations and facilitate waste management [17, 18]. Chemically, calcium sulfate dihydrate reacted with tricalcium aluminate to form ettringite, creating a protective film that retarded the hydration process [19]. Although industrial by-products occasionally required processing to ensure compatibility, they effectively regulated setting times without compromising compressive strength, a performance metric influenced by their degree of dehydration [18, 20]. Research indicated that while the standard dosage ranged from 3.0% to 5.0%, a 5.5% addition proved optimal for specific Portland cements [21]. In contrast, deviations resulted in adverse effects on water demand, setting characteristics, and volumetric stability.

This study was motivated by the massive accumulation of by-product gypsum from the petrochemical industry, which poses significant environmental management challenges. While CLSM is recognized for its high tolerance for incorporating diverse industrial wastes, existing literature predominantly focuses on gypsum as a minor chemical additive or set retarder, fundamentally limiting its consumption volume. There remains a significant research gap regarding the bulk valorization of petrochemical-derived gypsum (PDG). Therefore, this research aimed to evaluate the feasibility of utilizing PDG as a functional aggregate substitute in CLSM. This approach not only addresses the pressing environmental need for large-scale PDG management but also surpasses conventional dosage limitations to develop sustainable, high-volume alternatives to natural aggregates. Because gypsum-rich cementitious systems are typically highly moisture-sensitive, evaluating their durability in aggressive aqueous environments is critical. Seawater immersion tests were thus conducted to investigate whether the common ion effect could uniquely stabilize the PDG matrix, thereby justifying its targeted application in sustainable coastal infrastructure. Concurrently, because substituting inert aggregates with reactive PDG fundamentally alters the binder's hydration kinetics, microstructural analyses, including scanning electron microscopy (SEM), X-ray diffraction (XRD), X-ray fluorescence (XRF), and thermogravimetric analysis (TGA), were essential. These techniques were employed to elucidate the complex sulfate activation mechanisms, trace the formation and stability of ettringite, and correlate these micro-level phase evolutions with the macroscopic engineering performance of the PDG-based CLSM.

## 2 Experimental methods

### 2.1 Materials

Three primary binders, Portland type I cement, fly ash, and PDG, were evaluated through physical and chemical testing to establish baseline properties. The cement binder exhibited a specific gravity of 3.15 and a Blaine fineness of 3690 $cm^2/g$, confirming its standard commercial quality. The fly ash, obtained from coal combustion, had a lower specific gravity of 2.25 and a high specific surface area of 5860 $cm^2/g$. Its chemical composition was dominated by silica (39.16%) and alumina (40.01%), with a low CaO content (7.26%), confirming its classification as Class F and its reliance on external calcium sources for pozzolanic activation.

The PDG, derived from the combustion of petroleum coke and subsequently hydrated, appeared as grayish-white, angular particles. After processing, the material was separated into coarse (4.75 to 9.53 mm) and fine (≤4.75 mm) fractions. The material possessed a specific gravity of 2.08 and a fineness modulus of 3.58 for the fine fraction. The specific surface area of PDG powder passing through a 200-mesh sieve (0.075 mm) is 3610 $cm^2/g$. Chemical analysis of PDG indicated the presence of sulfates, carbonates, and hydroxides, with notably high concentrations of calcium sulfate dihydrate (47.90%), calcium hydroxide (21.64%) and calcium oxide (5.82%). The XRF analysis (Table 1) revealed that the PDG

Table 1 **Chemical compositions of the raw materials (%)**

| Raw materials | Chemical compound | | | | | | | |
|---|---|---|---|---|---|---|---|---|
| | $Al_2O_3$ | $SiO_2$ | CaO | $Fe_2O_3$ | $SO_3$ | $Na_2O$ | MgO | other |
| Cement | 4.78 | 21.24 | 62.59 | 3.27 | 2.27 | 0.38 | 2.53 | 2.94 |
| Fly ash | 40.01 | 39.16 | 7.26 | 5.71 | 1.06 | 0.61 | 1.42 | 4.77 |
| PDG | 7.75 | 7.08 | 61.57 | 1.21 | 20.35 | 0.08 | 0.78 | 1.18 |

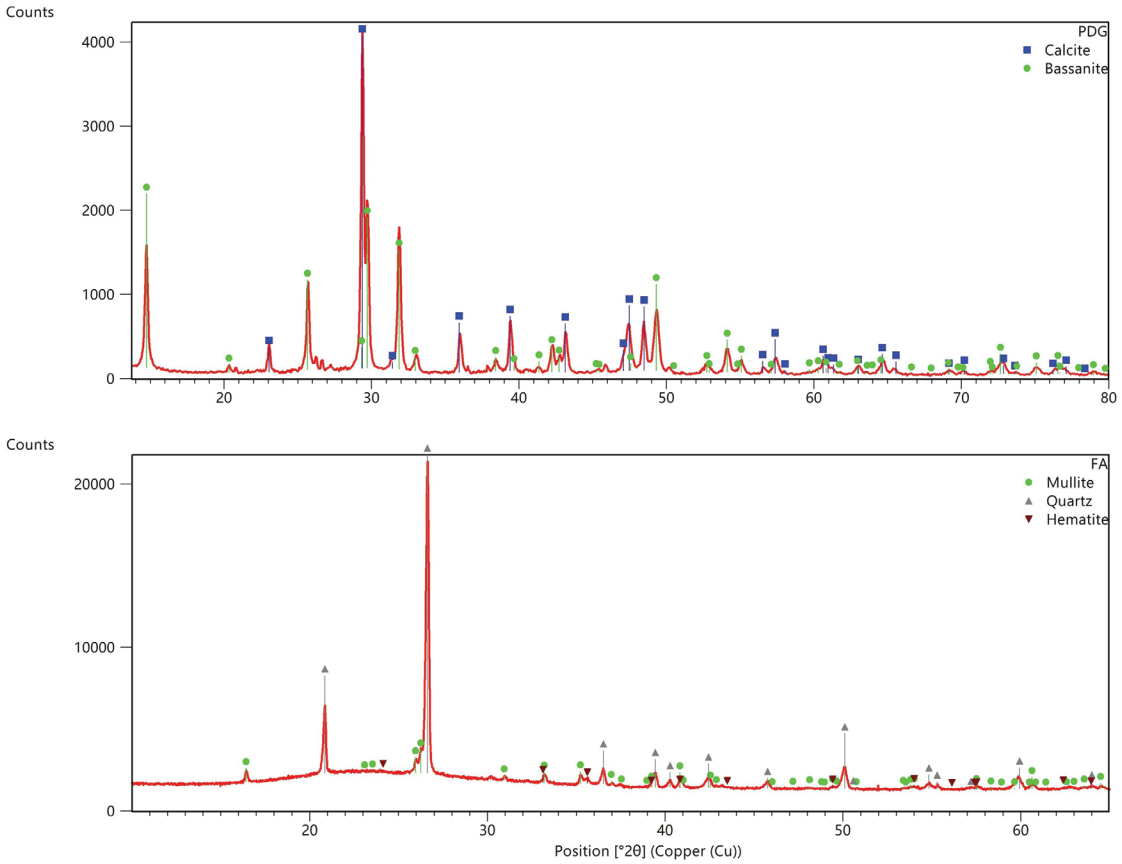


Figure 1 XRD patterns of petrochemical-derived gypsum (PDG) and fly ash (FA)

was predominantly composed of CaO (61.57%) and $SO_3$ (20.35%), confirming its high sulfate content, which is suitable for acting as a chemical activator. Furthermore, the XRD patterns (Figure 1) indicated that the fly ash comprised broad amorphous humps alongside crystalline quartz, mullite and hematite, whereas the PDG exhibited stable crystalline phases consistent with calcite and bassanite. These initial chemical and mineralogical characterizations thoroughly justified the observed microstructural behaviors in the later stages of hydration.

A single large batch of PDG was procured from a local recycling facility and used for all testing programs in this study to eliminate the influence of batch-to-batch compositional variations and ensure the internal reproducibility of the experimental results.

Furthermore, coarse and fine aggregates were procured from the Lanyang River in Taiwan. The specific gravity was determined to be 2.60, with fineness moduli of 2.59 and 6.62 for the fine and coarse aggregates, respectively, and water absorption rates of 1.10% and 1.15%. The seawater utilized for the testing was collected from the coastal region of Zhuangwei Township, Yilan County, Taiwan.

## 2.2 Mix proportion

The experimental program was designed as a two-stage practical engineering case study specifically targeted at utilizing the material for seawall and river embankment core applications, rather than a traditional continuous parametric variation study. Because the selected mix proportions were based on established industrial applications, their fresh properties (e.g., flow, bleeding, and setting time) had been pre-validated by the concrete manufacturer to meet standard construction criteria. Therefore, the experimental scope of this study specifically focused on an in-depth evaluation of the hardened mechanical properties, microstructural evolution, and environmental durability of the PDG-based CLSM. Weight-based replacement was selected over volumetric replacement to align with standard industrial batching operations for CLSM and to ensure accurate control of mixture proportions, accounting for the different specific gravities of PDG and natural aggregates. Stage I evaluated the theoretical maximum limit of waste utilization by completely replacing natural aggregates with PDG. A water-to-binder ratio (w/b) of 0.750 was empirically selected to address the high water absorption and angular characteristics of the 100% PDG aggregate system while maintaining sufficient flowability. The PDG aggregates were prepared to include 20% of particles between 4.75 mm and 9.53 mm, with the remaining 80% smaller than 4.75 mm. Based on the findings from Stage I, Stage II optimized the formulations for actual industrial implementation. Mixes B and C (37% and 50% PDG replacement, respectively)

Table 2 **Mix proportions and design parameters (kg/m³)**

| Mix no. | w/b | Water | Cement | Fly ash | PDG* | Fine aggregates** | Coarse aggregates** |
|---|---|---|---|---|---|---|---|
| | Stage I (100% PDG replacement) | | | | | | |
| A | 0.750 | 225 | 200 | 100 | 1120 | 0 | 0 |
| | Stage II (Partial replacement by PDG) | | | | | | |
| B | 0.865 | 225 | 136 | 124 | 578 | 267 | 268 |
| C | 0.865 | 225 | 152 | 108 | 813 | 0 | 337 |

Notes: On mix design parameters: Moisture state: All PDG and natural aggregates were prepared and incorporated into the mixtures in a Saturated-Surface-Dry (SSD) state to strictly control the effective w/b. *Gradation of PDG: The processed PDG aggregates were specifically graded to contain 20% coarse particles (4.75 mm to 9.53 mm) and 80% fine particles (≤4.75 mm). **Gradation of natural aggregates: Fine aggregates had a fineness modulus of 2.59, and coarse aggregates had a fineness modulus of 6.62 (maximum nominal size of 9.53 mm).

were not designed as sequential parametric variables; rather, they directly replicated two specific, standard CLSM proportions currently utilized in Taiwanese coastal engineering practice. Mix B evaluated a well-graded substitution (replacing portions of both fine and coarse aggregates), while Mix C represented a gap-graded scenario (fully replacing natural fine aggregates). The w/b was consequently adjusted to 0.865 to align precisely with these established practical engineering standards for seawall core applications. The detailed mix proportions are summarized in Table 2.

### 2.3 Test methods

For stage I, the specimen mixing procedure was performed in accordance with ASTM D4832, and the curing conditions for the 5 cm cubic specimens were compared under both water-curing and air-curing conditions. Compressive strength testing was conducted in accordance with ASTM C109 protocols. Specimens were cast as 5 cm cubes and tested at 7, 14, and 28 days to confirm that strength values remained below the CLSM specification limit of 8.3 MPa [22]. Five replicate specimens were evaluated for each mixture, and the average and standard deviation were recorded to assess statistical significance (error bars represent the standard deviation of five replicate test results). For the drying shrinkage test, prismatic specimens measuring 2.5 × 2.5 × 28.5 cm were prepared in accordance with ASTM C596. These specimens were maintained under atmospheric curing conditions, with measurements collected at 7, 14, 28, 56, 91, 180, and 365 days. Data were averaged from ten specimens.

Additionally, specimens cured in air for 28 days were divided into two groups: five specimens were immersed in tap water for 28 days, and five in seawater, before undergoing compressive strength testing. The remaining specimens were immersed in tap water and air for 100 days, after which specimens were collected for XRD, XRF, and TGA analyses. For SEM testing, 1 × 1 × 10 mm fragments were selected and processed according to ASTM C1723 procedures and it focused on specimens immersed in seawater and tap water for up to 100 days. For XRD and XRF analysis, 5 g of powder was collected for each test. To obtain these representative samples, fragments were extracted from the interior core of the crushed specimens after compressive strength testing and subsequently ground manually into a fine powder. The samples were then examined in accordance with ASTM C1356 and ASTM C114, respectively. Similarly, 5 g of the manually ground powder was used for TGA testing and analyzed in accordance with ASTM C1872.

The stage II of testing utilized 5 cm cubic specimens. After demolding, all specimens were subjected to air curing conditions (temperature of 25 ± 2°C and relative humidity of 50 ± 5%) until the designated testing age, and compressive strength tests were performed after 28 days. The specimens were subsequently separated into five groups: PDG particles, intact specimens immersed in seawater and tap water, and fragmented specimens immersed in seawater and tap water, forming a total of five groups. After 28 days of air curing, these specimens were placed in the designated environments for immersion testing. The immersion period extended for 60 days. Samples were collected from the immersion solutions at 10, 20, 40, and 60 days for testing and analysis. Parameters assessed included pH, sulphate, chloride ions and 11 heavy metals (cadmium, hexavalent chromium, copper, nickel, lead, zinc, silver, manganese, arsenic and selenium, and mercury). The seawater immersion test was conducted in accordance with the NIEA R220.20C standard (Test Method for Marine Environmental Leaching, Taiwan) [23], utilizing a fixed solid-to-liquid ratio of 0.029 (by weight) at a controlled temperature of [25 ± 2°C]. Specimens were first air-cured for 28 days and subsequently immersed in the seawater collected off the coast of Yilan, Taiwan, for the specified duration. To accurately simulate a static marine environment and maintain the initial chemical exposure, seawater was not replenished during the testing period; instead, the immersion containers were carefully surface-sealed to prevent further water evaporation. To standardize the strength reporting, the softening coefficient was calculated for all immersed specimens by dividing the residual compressive strength after

immersion by the 28-day air-cured compressive strength.

pH was measured using a handheld meter; sulphate and chloride ions were determined via titration apparatus, while heavy metals were evaluated using inductively coupled plasma-mass spectrometry (ICP-MS). Each sampling consisted of 10 mL of leachate to support testing. The leachate test results provide a reference for evaluating the environmental impact of future CLSM applications in practical seawall engineering projects.

## 3 Results and discussion

### 3.1 Compressive strength for stage I

Figure 2 illustrates the compressive strength development measured at 7, 14, and 28 days, demonstrating a progressive increase of approximately 2.04 MPa at 7 days, 2.65 MPa at 14 days, and 4.69 MPa at 28 days, respectively. The material achieved a strength of 2.04 MPa within the first week. This initial strength was primarily attributed to the hydration of the alite ($C_3S$) phase in the Portland cement. Despite the retarding effect of high sulfate concentrations (which can coat cement grains), the cement content of 200 kg/m³ was sufficient to establish a rigid skeletal framework. The 2.04 MPa value is notably high for CLSM; typically, 7-day strengths for excavatable fills are below 0.5 MPa [22, 24]. It suggested that the PDG aggregate might have acted as a nucleation site for hydration products, thereby accelerating the early formation of structure. A moderate increase of approximately 30% was observed, resulting in a strength of 2.65 MPa. During this phase, the hydration of $C_3S$ continued, and the formation of secondary ettringite likely began to densify the interfacial transition zone between the binder paste and the gypsum aggregate surfaces [25]. A notable observation was the continued strength development between 14 and 28 days, where the compressive strength increased by nearly 77% (from 2.65 to 4.69 MPa). This steep acceleration is characteristic of the pozzolanic reaction of class F fly ash. As alkalinity built up in the pore solution, the dissolution of the fly ash glass phase accelerated, producing secondary calcium silicate hydrate (C-S-H) gel that filled capillary pores. Furthermore, the synergistic interaction between the aluminates in the fly ash and the sulfates from the PDG likely led to a sustained formation of ettringite, further interlocking the matrix [26]. The final strength of 4.69 MPa represents a highly consolidated material.

In conventional concrete, the sulfate source is limited (3–5% gypsum). Once consumed, ettringite converts to monosulfate. In this PDG-CLSM, the infinite reservoir of sulfate from the aggregate ensured that ettringite remained the stable phase [27]. The continuous growth of needle-like ettringite crystals within the paste and at the aggregate interface facilitated microstructural densification at the micro-scale, contributing to the high compressive strength observed. Besides, the fly ash served a dual purpose. It provided the silica for C-S-H formation and the alumina for ettringite formation. The results clearly showed that the fly ash effect was delayed, manifesting most strongly after 14 days, consistent with the literature on high-volume fly ash systems [28].

According to ASTM standards and ACI Committee 229 guidelines, CLSM was defined as a self-consolidating cementitious material with unconfined compressive strength not exceeding 8.3 MPa at 28 days. The 28-day compressive strength of 4.65 MPa satisfied this upper threshold, confirming the material's classification as CLSM. Given that the measured strength substantially exceeded the typical 2.1 MPa upper limit for excavatable mixtures, the PDG-based mixture was explicitly positioned as a structural backfill suitable for load-bearing applications [29]. The measured 28-day strength of 4.65 MPa substantially exceeded conventional excavatable limits, indicating that the PDG-based mixture was more suitable for structural fill applications. In contrast to

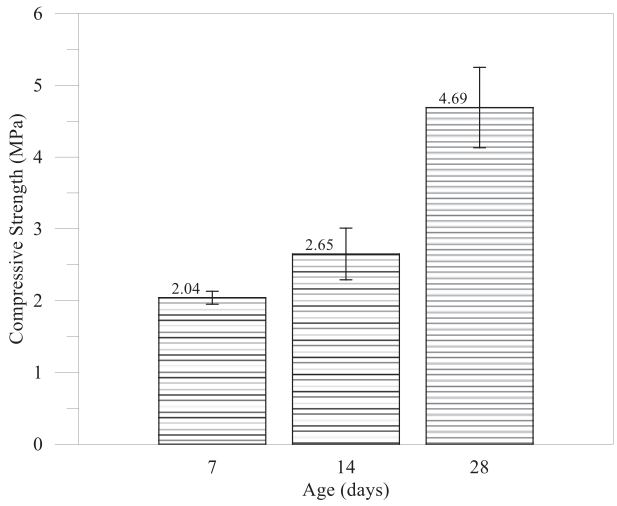


Figure 2 Compressive strength histograms for Stage I

other waste gypsums (e.g., titanium gypsum) that reduce late-stage strength to favor excavatability, the PDG investigated in this study uniquely functioned as an active strength enhancer, specifically positioning it for load-bearing infrastructure applications. Gui investigated a CLSM using organic muck and phosphogypsum [30]. Their optimal mixes achieved strengths in the range of 0.3 to 1.8 MPa. The higher strength in the current study (4.69 MPa) suggests that petrochemical gypsum may have better mechanical properties (particle hardness) or fewer deleterious impurities (such as phosphates or organics) than the materials used by Gui. It underscores the variability of waste gypsum and the need for source-specific mix design.

### 3.2 Length variation

The results of length variation measurements from 7 days to 365 days are shown in Figure 3. It corresponded to cumulative shrinkage strains ranging from 400 microstrain at an early age to 1100 microstrain at one year. While this indicated some volumetric change characteristic of cementitious materials lacking conventional aggregate restraint, the overall drying shrinkage of 0.11% over 365 days was considered relatively low for CLSM. Additionally, the porous physical properties of the alternative aggregates significantly influenced the evolution of internal relative humidity and moisture diffusion, a mechanism similarly observed in other recycled aggregate systems [31]. Comparative analysis with the literature revealed that the 28-day shrinkage of 0.06% (579 microstrain) and the 365-day shrinkage of 0.11% (1097 microstrain) positioned this PDG-based CLSM within the range of conventional cement mortar systems but exceeded the values reported for gypsum-modified materials designed for shrinkage reduction. Chen demonstrated that the incorporation of combined fly ash and gypsum reduced drying shrinkage by 25.3% while enhancing compressive strength [32]. Hanjitsuwan utilized FGD-gypsum and dolomite as expansive additives in alkali-activated high-calcium fly ash, effectively improving drying shrinkage resistance through engineered expansive reactions [33]. Xue reported that incorporating desulfurized gypsum into alkali-activated slag and hybrid alkali-activated cement reduced both autogenous and drying shrinkage more effectively than normal gypsum, attributed to higher Ca/Si ratios in the gel phases, optimized crystalline-to-gel phase ratios, and favorable pore structure modifications [34].

From another perspective, a drying shrinkage of 0.11% over 365 days was considered relatively low for CLSM. The research investigated the use of recycled gypsum from construction and demolition waste [35]. The findings mirrored the results of this study that the inclusion of gypsum (up to 20 to 40%) reduced shrinkage cracking. However, they noted that the source of gypsum (fine vs. coarse) influenced water demand. The current use of PDG in this study, which typically has a finer and more uniform particle size distribution than crushed drywall, likely provided better reactivity control, as evidenced by the consistent 365-day stability. Literature on red gypsum utilized in CLSM reported shrinkage values in the range of 0.02% to 0.05%, which is considered negligible for backfill applications [36]. The PDG-based CLSM in this study contrasted favorably with conventional soil-cement or pure cement-fly ash CLSMs, which can exhibit shrinkage an order of magnitude higher due to the lack of chemical compensation mechanisms.

### 3.3 Immersion test and microstructures

After curing specimens for 28 days, the specimens were subsequently immersed in natural seawater and tap water, respectively, for a further 28 days (thus completing 56 days of curing). The specimens were then removed and subjected to compressive strength testing, with the results shown

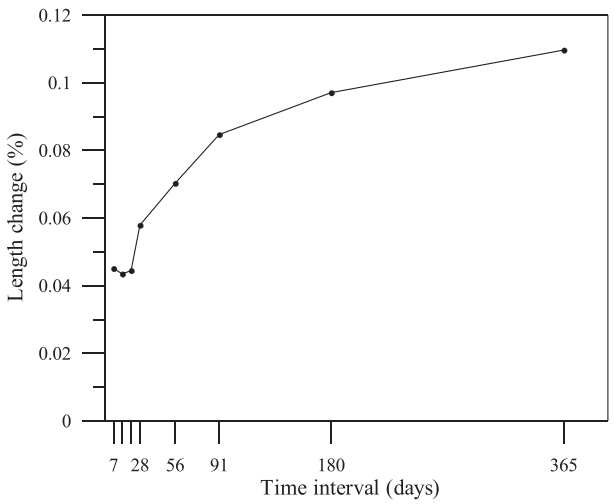


Figure 3 Length change curves

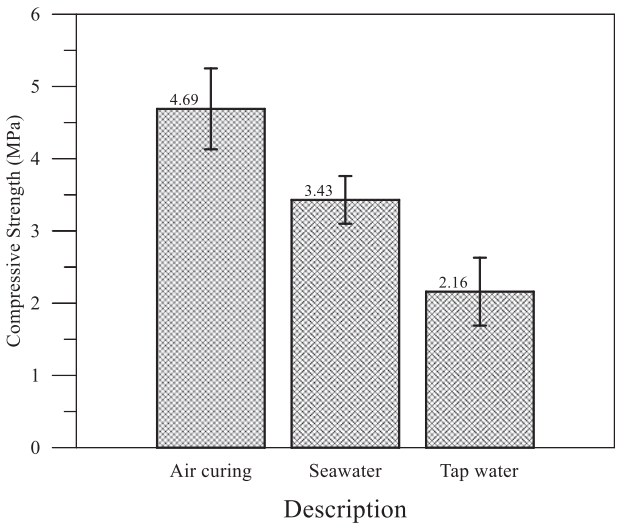


**Figure 4** Strength histograms after immersion test

in Figure 4. The PDG-based CLSM exhibited substantial strength degradation upon water immersion, with tap water causing a 54% reduction and seawater a 27% reduction relative to the 28-day air-cured strength. The decrease in strength upon wetting is quantified by the softening coefficient, a standard durability index for gypsum-based materials [37]. The softening coefficients were calculated by dividing the compressive strength after immersion in solution by the compressive strength before immersion. The softening coefficients of 0.46 and 0.73, respectively, indicated poor to moderate water resistance substantially below acceptable thresholds. The superior performance in seawater compared to tap water, attributable to common ion effects limiting gypsum dissolution, protective chloride-based precipitates, and reduced water activity, contrasted with typical concrete deterioration patterns and highlighted the dominance of dissolution mechanisms in gypsum-rich systems. These findings demonstrate that the durability of PDG-based CLSM is highly environment-dependent. While the common-ion effect uniquely stabilizes the material in marine environments, making it suitable for coastal applications, exposure to freshwater poses a significant risk of structural degradation. Consequently, caution must be exercised, and PDG-based CLSM should not be applied in freshwater-exposed environments without implementing additional waterproofing strategies.

Tap water serves as a solvent characterized by very low ionic strength and negligible concentrations of calcium ($Ca^{2+}$) and sulfate ($SO_4^{2-}$) ions. Upon the submersion of the PDG-based CLSM, a notable concentration gradient developed between the saturated pore solution, which maintains an equilibrium gypsum concentration of approximately 15 mmol/L, and the surrounding bulk water [38]. In addition to gypsum dissolution, this freshwater environment facilitated the leaching of Portlandite ($Ca(OH)_2$). The subsequent depletion of $Ca(OH)_2$ resulted in a reduction of the pore solution's pH. Because high alkalinity is a prerequisite for stabilizing C-S-H gel, the decreasing pH caused the gel to undergo decalcification; this process transformed the material from a rigid gel with a high Ca/Si ratio into a porous silica gel characterized by a low Ca/Si ratio and minimal binding strength [39]. The cumulative impact of gypsum dissolution and binder leaching resulted in microstructural disintegration. A recent investigation [40] by Lin noted that waste gypsum CLSM specimens immersed in water displayed surface cracking, spalling, and eventual disintegration, phenomena that align with the severe strength loss recorded in Mix A. Fundamentally, the tap water compromised the structural integrity of the composite.

In standard reinforced concrete, seawater serves as a highly aggressive agent that induces chloride corrosion and sulfate attack. Conversely, for a gypsum-based matrix, seawater functions as a stabilizing environment attributable to the common ion effect. In freshwater settings, ettringite is unstable and prone to decomposition as sulfate ions leach from the material. However, the elevated background concentration of sulfate in seawater stabilizes the ettringite crystals, effectively preventing their dissolution. As ettringite contributes to the structural framework of the CLSM, established during the air curing phase, its preservation in seawater directly correlates with the observed higher compressive strength of 3.43 MPa. Research by Li et al. [41] and Cai et al. [42] confirms that seawater curing facilitates a denser microstructure through this mechanism, resulting in greater residual strength compared to freshwater curing.

To establish the baseline hydration mechanism of the fully replaced system, the SEM micrograph of Mix A (100% PDG replacement from Stage I) at 91 days (Figure 5) was evaluated. It revealed a highly dense microstructure characterized by an

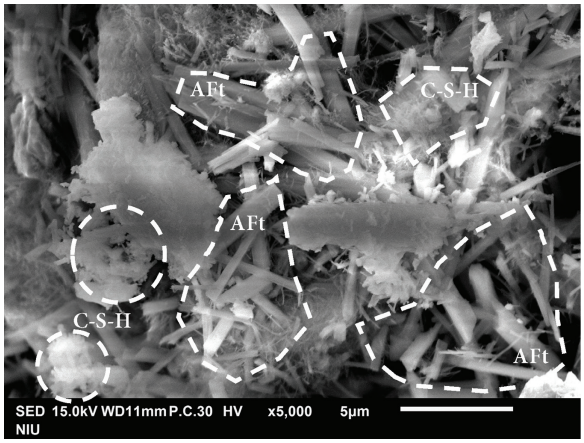


Figure 5 SEM photo at 91 days for Mix A (×5000)

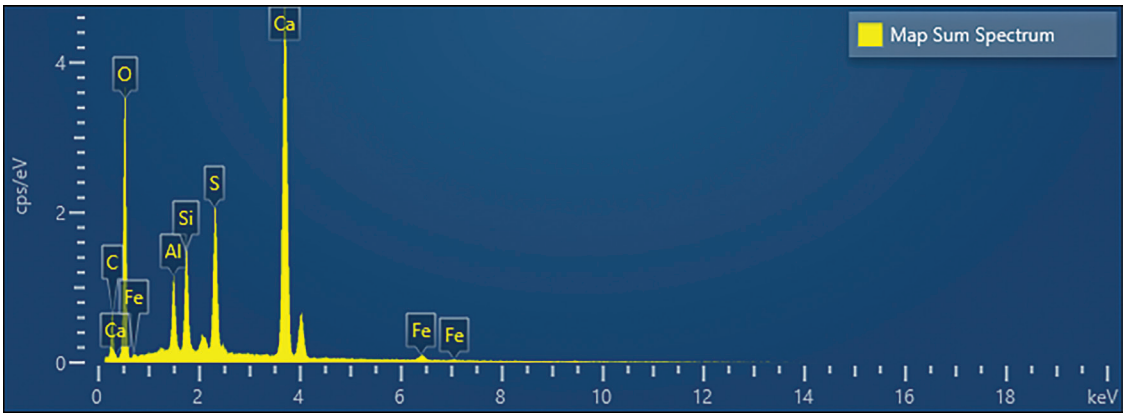


Figure 6 EDS results from Figure 5

extensive network of needle-like crystals filling the capillary voids and bridging the aggregate particles. Energy dispersive spectroscopy (EDS) analysis (Figure 6 and Table 3) confirmed the elemental composition of these crystals, showing predominant peaks for calcium (Ca), sulfur (S), aluminum (Al), and oxygen (O). This elemental signature is characteristic of calcium sulfoaluminate hydrates, specifically AFt. The presence of silicon (Si) peaks in the spectrum further indicated the coexistence of C-S-H gel, likely formed through the pozzolanic reaction of the fly ash, which coated the inert PDG particles and provided additional binding sites.

The XRD patterns (Figure 7) corroborated the SEM/EDS findings, identifying ettringite as the dominant crystalline phase (intensity > 10,000 counts). The detection of residual gypsum and calcite indicated that while the PDG acted as a reactive aggregate, a portion remained to provide a stable skeletal framework. The breakdown of phases suggests a specific hydration pathway where the PDG acted as an *in-situ* sulfate activator.

Table 3 Results of elemental analysis by EDS

| Map Sum Spectrum | | | | |
|---|---|---|---|---|
| **Element** | **Line Type** | **Weight %** | **Weight % sigma** | **Atomic %** |
| O | K series | 46.49 | 0.34 | 60.15 |
| A1 | K series | 2.64 | 0.06 | 2.03 |
| Si | K series | 3.75 | 0.07 | 2.76 |
| S | K series | 7.13 | 0.10 | 4.60 |
| Ca | K series | 30.25 | 0.24 | 15.62 |
| Fe | K series | 1.43 | 0.14 | 0.53 |
| C | K series | 8.30 | 0.32 | 14.31 |
| Total | | 100.00 | | 100.00 |

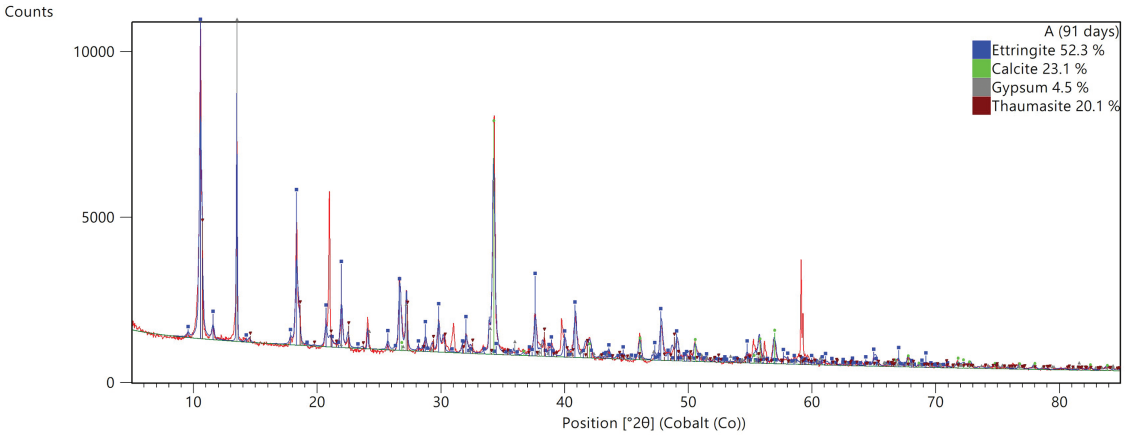


Figure 7 **XRD patterns**

The PDG provided a continuous supply of sulfate ions ($SO_4^{2-}$) into the pore solution. These ions reacted with the tricalcium aluminate ($C_3A$) from the cement and the reactive alumina ($Al_2O_3$) released by the glass phase of the fly ash [43] as follows:

$$6Ca^{2+}_{(aq)} + 2Al(OH)^{-}_{4(aq)} + 3SO^{2-}_{4\ (aq)} + 4OH^{-}_{(aq)} + 26H_2O_{(l)} \rightarrow 3CaO \cdot Al_2O_3 \cdot 3CaSO_4 \cdot 32H_2O_{(s)}$$
$$(ettringite)$$

Unlike conventional CLSM, where aggregates are inert, the PDG actively participated in hydration. The massive precipitation of ettringite needles filled voids and interlocked the matrix, which directly contributed to the high long-term strength observed in previous sections.

These findings align with recent studies on the valorization of sulfate-rich waste. Gui et al. [30] reported that in phosphogypsum-based binders, the synergistic activation of fly ash by sulfate ions is the primary driver for densification, forming a skeleton-filling structure of AFt and C-S-H. Similarly, previous research [40, 44] has observed that sufficient sulfate availability is crucial for stabilizing ettringite in high-volume waste matrices, thereby preventing its conversion to monosulfate and ensuring dimensional stability. The microstructure observed in Mix A confirms that petrochemical gypsum serves effectively as a chemical reactant, surpassing inert sands in promoting specific hydrate growth for enhanced structural competence.

### 3.4 Effects of air curing and water curing

Utilizing the TGA results depicted in Figure 8, the thermal stability and hydration product evolution of the CLSM mixture comprising PDG were examined at the age of 100 days. Classification based on previous literature [45], the decomposition phases were identified beginning with the 105°C to 200°C range, which involved the dehydration of C-S-H gel and ettringite alongside the phase transformation of residual gypsum

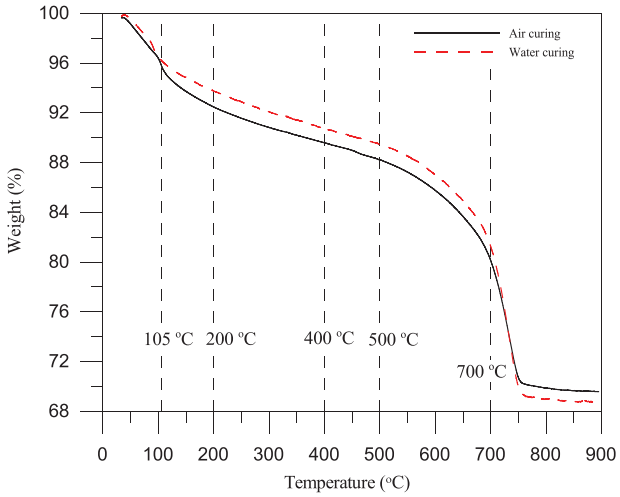


Figure 8 **TGA curves**

from dihydrate to hemihydrate. Subsequently, the decomposition of calcium aluminate hydrates (C-A-H) and monosulfate (AFm) was observed between 200°C and 400°C. It was followed by the dehydroxylation of calcium hydroxide (CH) from 400°C to 500°C, and finally, the decarbonation of calcium carbonate ($CaCO_3$) occurred between 500°C and 700°C.

TGA curves revealed a notable divergence between the curing regimes. The air-cured specimen (black line) exhibited a noticeably greater mass loss in the critical 105 to 400°C range compared to the water-cured specimen (red line). This increased mass loss indicated a higher concentration of C-S-H gel and ettringite in the air-cured matrix. The PDG actively participated in the hydration process by supplying sulfate ions ($SO_4^{2-}$), which reacted with the aluminates from the fly ash and cement to form extensive needle-like ettringite crystals [28]. This reaction densified the microstructure, contributing to the superior strength observed in air-cured samples. Conversely, the water-cured specimen showed reduced mass loss in these regions, implying a lower content of stable hydration products. This reduction was attributed to the high solubility of the gypsum-based matrix. Water immersion likely caused the dissolution of the gypsum skeleton and the leaching of calcium and sulfate ions, destabilizing the ettringite and C-S-H network [46]. The substantial mass loss observed in both samples above 600°C confirmed the presence of calcite, an inherent impurity in the waste PDG, which remained stable up to high temperatures. The TGA results ultimately confirmed that PDG acted as an effective sulfate activator for ettringite and C-S-H formation under air curing but suffered from chemical instability and leaching when submerged [47].

### 3.5 SEM observation

Based on the microstructural and mineralogical analyses presented in Figures 9–12, the microstructural evidence was explicitly linked to the observed macroscopic mechanical trends. The SEM micrograph of the air-cured specimen revealed a dense and cohesive microstructure characterized by a proliferation of needle-like ettringite (AFt) crystals bridging the PDG particles. This dense interlocking network, resulting from the PDG acting as an *in-situ* sulfate activator ($C_3A + 3C\bar{S}H_2 \rightarrow C_6A\bar{S}_3H_{32}$), directly accounted for the high 28-day compressive strength and drove the distinct air-hardening mechanism [48]. Conversely, the water-cured specimen exhibited a loose and granular morphology with significant voids resulting from the dissolution of the soluble gypsum matrix and metastable ettringite. Corroborating these observations, the XRD patterns indicated that the water-cured sample was dominated by inert calcite (76.2%) and bassanite (22.6%) with a notable absence of distinct ettringite peaks. This severe microstructural degradation provided a definitive mechanistic explanation for the substantial strength loss and low softening coefficients observed during the immersion tests, confirming that while PDG enhances strength in dry conditions, it leads to structural collapse in moisture-rich environments.

In contrast, the air-cured specimen displayed a lower relative proportion of calcite (68.0%) alongside quartz and bassanite, confirming that the air-cured environment allowed the PDG-fly ash-cement system to reach a stable hydraulic equilibrium where C-S-H gel and AFt filled the voids [30, 47]. Ultimately, these findings confirm that while PDG serves as a reactive component that enhances strength through ettringite formation under air-cured conditions, it leads to microstructural collapse and strength loss in freshwater environments due to hydrodynamic instability. This finding is consistent with the previous results.

### 3.6 Engineering application: strength

Based on the findings from the preceding analysis, this study modified the SP mix by partially substituting coarse and fine aggregates, while reducing the PDG usage rate to 50% and 37%, as detailed in Table 2. The 28-day compressive strength of these three mix designs is illustrated

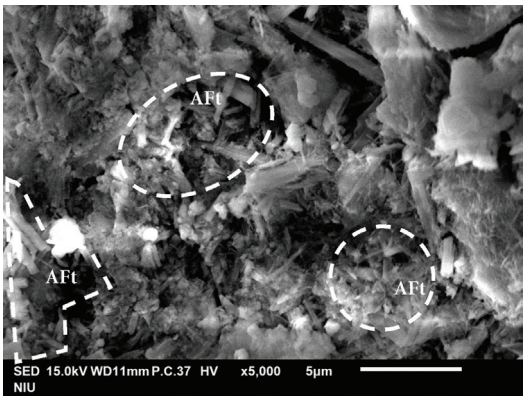


Figure 9 SEM photo under air-cured specimen (×5000)

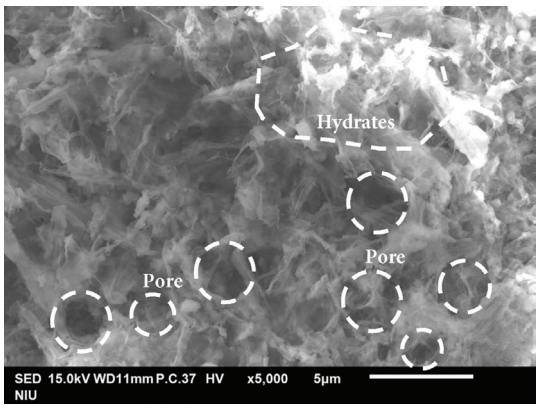


Figure 10 SEM photo under water-cured specimen (×5000)

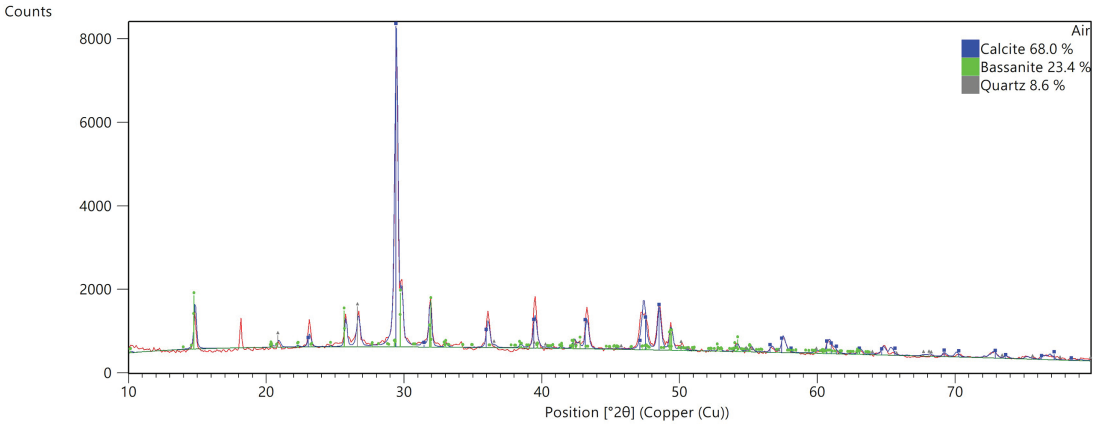


Figure 11 **XRD patterns under air-cured specimen**

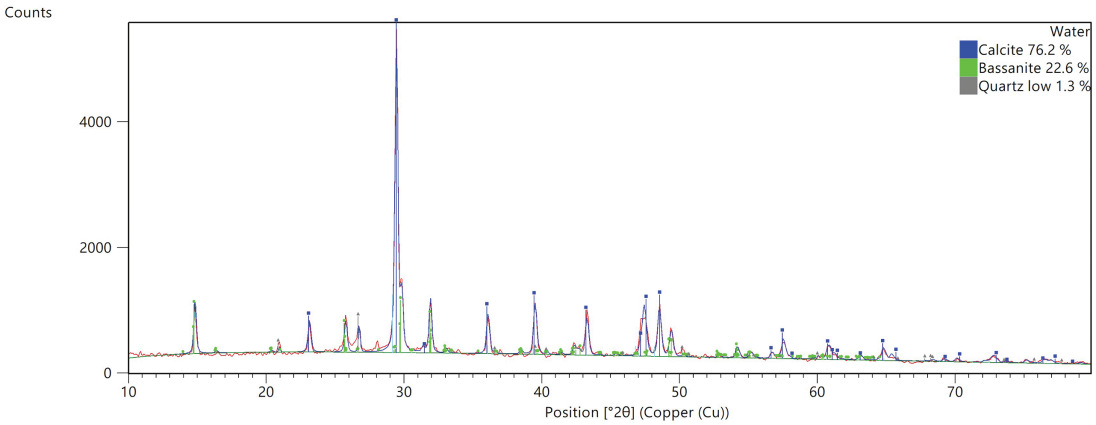


Figure 12 **XRD patterns under water-cured specimen**

in Figure 13, where Mix Designs B and C were adjusted to align with the CLSM mix proportions used in industrial practice in Taiwan.

Based on the compressive strength results presented in Figure 13 and the mix proportions in Table 2, the mechanical performance of the CLSM was significantly influenced by the petrochemical-derived gypsum replacement ratio and aggregate gradation. The data revealed that Mix B with 37% PDG achieved the highest 28-day compressive strength of 4.72 MPa, slightly outperforming the 4.69 MPa of the full replacement Mix A and the 4.23 MPa of Mix C, providing evidence that partial replacement is mechanically superior to full replacement. Notably, Mix B attained this peak performance despite containing significantly less

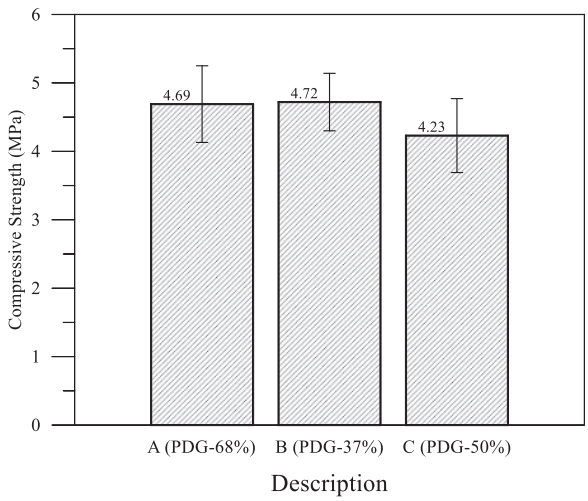


Figure 13 **Strength histograms between Stage I and Stage II**

cement at 136 kg/m³ compared to the 200 kg/m³ in Mix A, as the inclusion of natural sand and coarse aggregates created a denser skeletal structure with optimized particle packing. Within this optimized system, the PDG acted synergistically as both a filler and sulfate activator, promoting hydration products without generating the excessive void space associated with the angular particles found in the full replacement mix. This finding aligns with recent studies by Gui et al. and Zhang et al. [30, 47] regarding void ratio optimization. Conversely, the lowest strength observed in Mix C was attributed to the absence of natural fine aggregates, resulting in a gap-graded mixture with increased interparticle voids that weakened the matrix. Ultimately, all three mixes exceeded the ACI 229R upper threshold of 2.1 MPa, qualifying as structural fills. Yet, the superior efficiency of Mix B confirms that integrating petrochemical gypsum into standard industrial mix designs offers the most effective strategy for producing high-bearing capacity backfills with a reduced carbon footprint. This approach aligns with recent advancements in sustainable coastal construction, where integrating industrial wastes successfully reduced embodied carbon while maintaining mechanical integrity [48, 49].

Ultimately, with 28-day compressive strengths ranging from 4.23 to 4.72 MPa, all three mixes were explicitly classified as structural backfill, making them ideal for load-bearing applications such as road sub-bases and seawall cores. The superior efficiency of Mix B confirmed that integrating petrochemical gypsum into standard industrial mix designs was the most effective strategy for producing high-bearing-capacity structural fills with a reduced carbon footprint. Optimizing from 37% to 50% of PDG prioritized durability and reduced expansion risk over raw strength.

### 3.7 Engineering application: ion leaching

Based on the mix proportions in Table 2 and the seawater immersion pH test results in Figure 14. Five seawater-immersed specimens were prepared: PDG granules (No. 1), intact and fragmented samples of Mix B (No. 2 and No. 3), and intact and fragmented samples of Mix C (No. 4 and No. 5). The analysis of the five specimen groups reveals that PDG-based CLSM exhibits robust environmental stability, making it suitable for marine applications. The data demonstrate that raw PDG particles are chemically inert, maintaining a stable pH of 8.1–8.2, which closely aligns with the natural seawater baseline without inducing acidification or alkalinization. This stability extends to the intact CLSM cubes for both Mix B and Mix C, which maintained pH values between 8.2 and 8.5 due to the dense cementitious matrix effectively immobilizing alkaline hydration products and restricting ion diffusion. While increasing the surface area through crushing caused a rise in pH for Mix B and Mix C to approximately 9.2 and 9.8, respectively, these values stabilized below 10 and remained significantly lower than the typical pH of fresh concrete pore solution. The slightly higher pH observed in the crushed Mix C is directly attributable to its higher cement content of 152 kg/m³, generating more calcium hydroxide compared to the 136 kg/m³ in Mix B. The overall stabilization of pH, even in crushed states, confirms that the material is environmentally benign, a result of the natural buffering capacity of seawater, where magnesium ions react with leached hydroxyl ions to precipitate brucite and aragonite on the surface [50]. This self-sealing mechanism prevents the formation of hyper-alkaline plumes and ensures the material remains non-hazardous to marine ecosystems.

Based on the heavy metal leaching results presented in Figure 15, the toxicity characteristic leaching procedure analysis confirmed the environmental safety of the PDG-based CLSM across all five specimen groups. The concentrations of all monitored heavy metals, including Cr, Cu, Ni, Pb, Zn, Mn, As, and Se, were significantly lower than the regulatory ceilings specified by the Taiwan Ministry of Environment's NIEA R220.20C

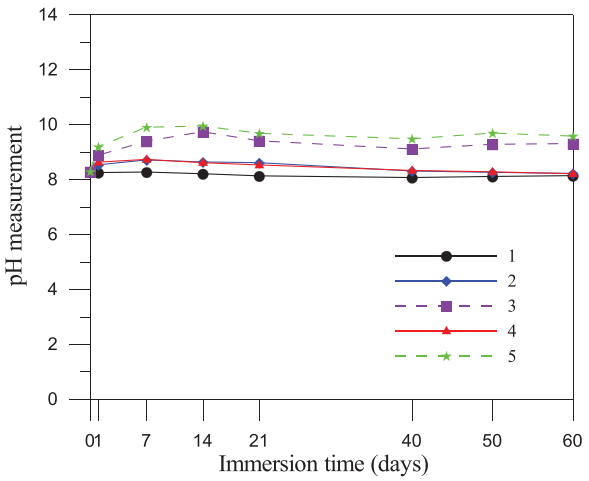


Figure 14 pH measurements

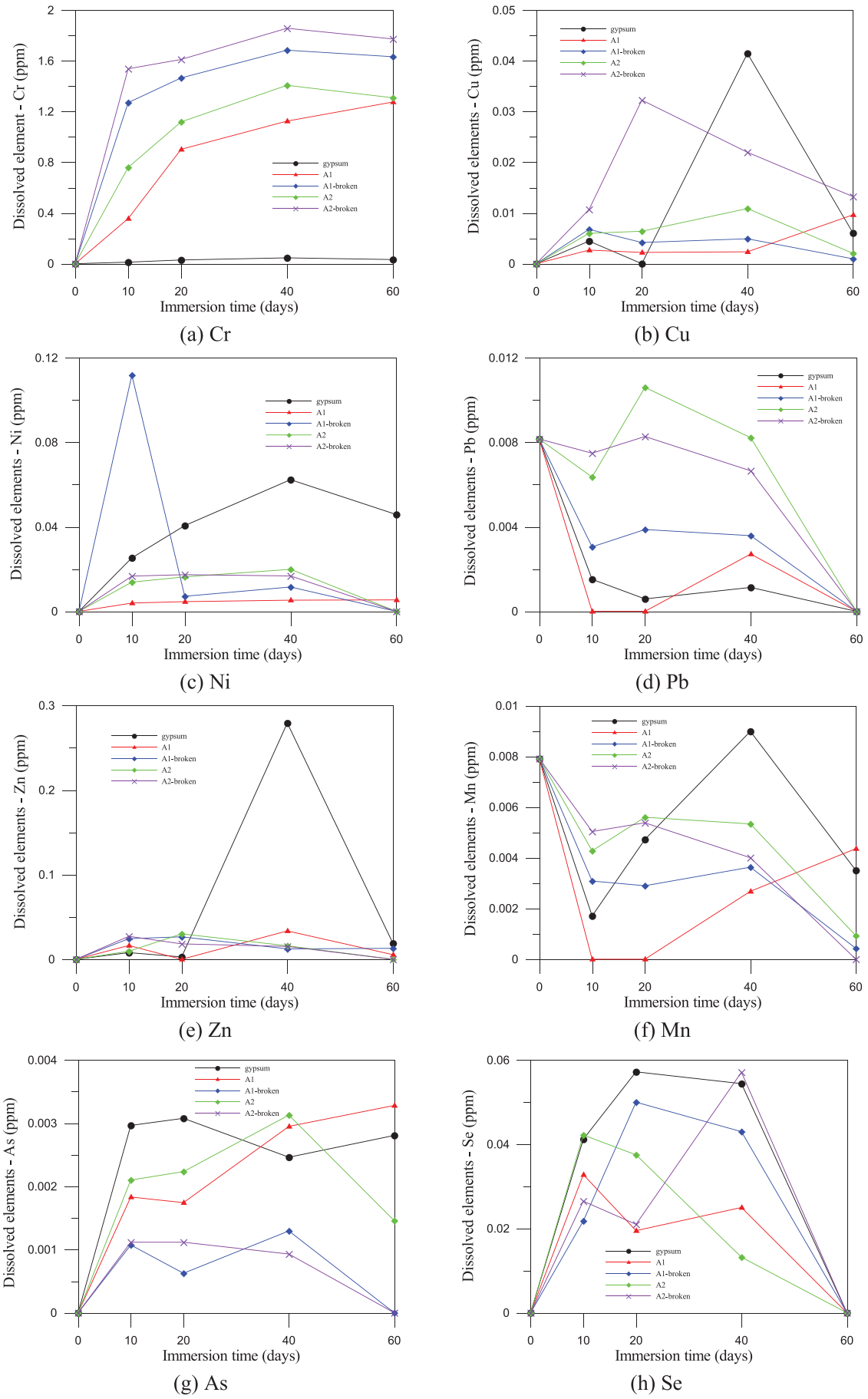


**Figure 15** Leaching test results for heavy metals

standard in Taiwan [23]. These local thresholds are generally consistent with international benchmarks, such as the United States Environmental Protection Agency (USEPA) Toxicity Characteristic Leaching Procedure (TCLP) limits (e.g., 5.0 mg/L for Cr, Pb, and As), thereby confirming the material's broad environmental compliance worldwide. Furthermore, elements such as Hg, Ag, and Cd remaining non-detectable. In contrast, others, such as Zn and Mn, appeared in negligible amounts. Although the increased surface area of crushed specimens in Groups 3 and 5 resulted in marginally higher leaching concentrations compared to the intact specimens of Groups 2 and 4, all values remained well within safe limits, indicating that the heavy metals were securely integrated into the material matrix rather than merely surface-bound. This robust environmental stability is attributed to the Solidification/Stabilization (S/S) mechanisms of the binary cement and fly ash binder system, where the formation of a dense C-S-H gel physically encapsulates ions, thereby restricting their mobility [51, 52]. At the same time, the high pH of the pore solution promotes chemical fixation through incorporation into hydration products or precipitation as insoluble hydroxides. Furthermore, the slightly alkaline nature of the seawater environment facilitates the maintenance of a stable state that prevents the re-dissolution of metal precipitates, thereby confirming that using PDG as either a full or partial aggregate replacement in CLSM meets stringent marine safety standards and poses no notable risk of heavy metal pollution. Additionally, the slight increase in concentration was caused by sampling 10 mL of solution each time, resulting in a reduction of 5 L of solution and consequently raising the solid-to-liquid ratio. In summary, the comprehensive analysis in this section established that while 100% PDG replacement achieved high compressive strength through ettringite formation, it was moisture-sensitive. By optimizing the mix to a 37% PDG partial replacement, the CLSM successfully balanced robust structural load-bearing capacity with excellent marine environmental stability, fully satisfying both engineering performance and regulatory safety requirements. Because the targeted practical applications for this PDG-based CLSM were permanent seawall and river embankment cores, manual excavation was not anticipated in the future. Therefore, the material was explicitly classified as a non-excavatable CLSM. According to ACI 229R guidelines, non-excavatable mixtures typically require a compressive strength exceeding 2.1 MPa to ensure adequate structural stability. The 28-day compressive strengths achieved in this study, ranging from 4.23 to 4.72 MPa, satisfied and exceeded this regulatory threshold, thereby thoroughly justifying the suitability of the developed PDG mixtures for high-bearing-capacity structural fill applications.

To comprehensively evaluate the environmental impact, the heavy metal leaching concentrations were systematically summarized and compared with the regulatory thresholds established by the Taiwan Environmental Protection Administration (EPA) and the corresponding method detection limits (summarized in Table 4). The leaching tests were conducted on crushed solid samples obtained from 28-day air-cured specimens, maintaining a fixed solid-to-liquid ratio of 0.029. The analytical results demonstrated that all target heavy metal concentrations were significantly below the strict regulatory thresholds, and several trace elements remained below the MDL. These summarized findings conclusively verified the environmental safety and chemical stability of the PDG-based CLSM for practical engineering applications.

The chemical stability of PDG-based CLSM in a marine environment was substantiated through the leaching analyses presented in Tables 5 and 6, which demonstrated excellent environmental compatibility relative to NIEA R220.20C regulatory

**Table 4** Corresponding method detection limits for heavy metals (ppm)

| Category | Cr | Cu | Ni | Pb | Zn | Mn | As | Se |
|---|---|---|---|---|---|---|---|---|
| Detection limits | 45 | 27 | 90 | 9 | 450 | 45 | 45 | 9 |

**Table 5** Results of sulphate leaching tests (mg/L)

| Mix no. | Dissolved sulphate content | | | | | |
|---|---|---|---|---|---|---|
| | 0 | 10 | 20 | 40 | 50 | 60 |
| 1 | 0 | ND | ND | ND | 20.5 | 39.5 |
| 2 | 0 | ND | ND | 3.5 | 15.5 | 26.3 |
| 3 | 0 | ND | ND | 21.0 | 23.8 | 31.3 |
| 4 | 0 | ND | ND | 2.0 | 23.5 | 26.3 |
| 5 | 0 | ND | ND | 11.5 | 26.5 | 28.0 |
| **Quality Control Standards <625 mg/L** | | | | | | |

Note: 1. Dissolved sulphate content = test value of sulphate concentration in seawater-immersed specimen solution—background value (seawater value); 2. Background value (seawater value) is 2716.5 mg/L; 3. ND indicates no detected.

Table 6 **Results of chloride ions leaching tests (mg/L)**

| Mix no. | Dissolved chloride ions content | | | | | |
|---|---|---|---|---|---|---|
| | 0 | 10 | 20 | 40 | 50 | 60 |
| 1 | 0 | ND | ND | 6.0 | 12.5 | 14.7 |
| 2 | 0 | ND | ND | ND | 9.0 | 16.0 |
| 3 | 0 | ND | ND | ND | 20.5 | 22.5 |
| 4 | 0 | ND | ND | ND | 8.7 | 15.0 |
| 5 | 0 | ND | ND | ND | 12.0 | 17.2 |
| **Quality Control Standards <240 mg/L** | | | | | | |

Note: 1. Dissolved chloride ions content = test value of chloride concentration in seawater-immersed specimen solution—background value (seawater value); 2. Background value (seawater value) is 23,131.3 mg/L; 3. ND indicates no detected.

standards [23] over a 60-day seawater immersion period. Specifically, dissolved sulfate concentrations were effectively immobilized by the binder system, ranging from 26.3 to 39.5 mg/L and remaining well below the 625 mg/L quality control limit. In contrast, chloride ion release remained minimal, at 14.7 to 22.5 mg/L, compared to the 240 mg/L regulatory cap. This robust resistance to leaching, consistently observed even in broken specimens, is attributed to Solidification/Stabilization mechanisms within the alkali-activated fly ash and cement matrix [52], which chemically fixate chloride and sulfate ions into stable phases, such as Friedel's salt and ettringite, respectively [53, 54]. Furthermore, physical encapsulation is achieved through the formation of a dense C-S-H gel and the subsequent precipitation of secondary minerals, such as brucite and aragonite, upon exposure to seawater, which densifies the pore structure to limit ion mobility strictly. This process confirms the compliance of PDG-based CLSM with Taiwan's environmental standards for sustainable marine infrastructure applications.

Despite the promising mechanical and microstructural performance observed up to 91 days, the long-term durability limits of the PDG-based CLSM remained an essential consideration for future engineering applications. Specifically, the inherently high sulfate content of the PDG posed a potential risk of delayed ettringite formation, which could, in theory, induce disruptive volumetric expansion over extended periods. Furthermore, while the mixtures exhibited stable early-age volume changes, long-term drying shrinkage and the progressive microstructural evolution beyond one year were not quantified in the current study. Consequently, subsequent extended-age research is strongly required to monitor these dimensional stability metrics, specifically focusing on rigorous shrinkage and sulfate expansion tests to validate the life-cycle durability of the proposed formulations comprehensively.

Based on a comprehensive synthesis of the mechanical, microstructural, and environmental evaluations conducted in this study, Mix B, with a 37% partial replacement of natural aggregates with PDG, was unequivocally identified as the optimal formulation for practical engineering applications. This mixture achieved an effective balance between the required structural bearing capacity, superior volumetric stability, and enhanced water resistance, while fully complying with marine environmental safety standards. A concise summary of its optimized mix proportions and corresponding key performance indicators (KPIs) was presented in Table 7, thereby providing a practical benchmark for future large-scale CLSM applications.

Table 7 **Recommended mix summary and KPIs**

| Category | Parameter | Optimized Specification (Mix B) |
|---|---|---|
| Mix proportions | Replacement ratio | 37% PDG (partial aggregate replacement) |
| | w/b | 0.865 |
| | Water (kg/m³) | 225 |
| | Cement (kg/m³) | 136 |
| | Fly ash (kg/m³) | 124 |
| | PDG aggregates (kg/m³) | 578 |
| | Fine aggregates (kg/m³) | 267 |
| | Coarse aggregates (kg/m³) | 268 |
| Key KPIs | Target CLSM classification | non-excavatable structural fill |
| | Compressive strength at 28 days | 4.72 MPa (exceeds 2.1 MPa ACI requirement) |
| | Seawater immersion | Softening Coefficient of 0.73 |
| | Environmental safety | 100% compliant with Taiwan EPA marine regulatory limits |
| | Chemical stability | stable pH (8.2–9.8); heavy metal leaching below limits |
| Primary application | | Seawall cores, river embankments, road sub-bases |

## 4 Conclusions

This research successfully validated the innovative application of PDG as a functional aggregate in CLSM, establishing a sustainable pathway for the large-scale valorization of industrial by-products. The key conclusions were drawn as follows:

1. Optimal replacement ratio: The optimized mixture incorporating a 37% PDG partial replacement attained a peak 28-day compressive strength of 4.72 MPa. It effectively synergized with fly ash to form an ettringite-reinforced matrix, ensuring an optimal balance among mechanical performance, volumetric stability, and waste utilization.
2. Durability limitations: While the PDG-based CLSM achieved high strength under air-curing conditions, it exhibited significant microstructural sensitivity and severe strength degradation in freshwater environments. Therefore, its long-term durability was highly environment-dependent, necessitating targeted application and avoiding direct freshwater exposure without waterproofing strategies.
3. Application potential: Leaching assessments confirmed that the material was ecologically safe, with heavy metal and pH levels well within marine regulatory limits. Consequently, the optimized 37% PDG mixture was positioned as a viable, high-bearing-capacity structural fill ideal for sustainable coastal infrastructure and road sub-base applications.


## Acknowledgement

Not applicable.

## Funding Statement

The authors want to acknowledge the National Science and Technology Council in Taiwan under Grant NSTC-114-2221-E-197-001-MY2.


## Author Contributions:

The authors confirm contribution to the paper as follows: Conceptualization, Jie Chen and An Cheng; methodology, Jie Chen and Wei-Ting Lin; validation, Kinga Korniejenko; investigation, An Cheng; resources, An Cheng and Wei-Ting Lin; data curation, Jie Chen and Kinga Korniejenko; writing—original draft preparation, Jie Chen and Wei-Ting Lin; writing—review and editing, Jie Chen and Wei-Ting Lin; visualization, Kinga Korniejenko; project administration, Wei-Ting Lin; funding acquisition, Wei-Ting Lin. All authors reviewed and approved the final version of the manuscript.

## Availability of Data and Materials

Not applicable.

## Ethics Approval

Not applicable.

## Conflicts of Interest

The authors declare no conflicts of interest.

REFERENCES


[1] Thorne J, Bompa DV, Funari MF, Garcia-Troncoso N. Environmental impact evaluation of low-carbon concrete incorporating fly ash and limestone. Clean Mater. 2024;12:100242. doi:10.1016/j.clema.2024.100242.
[2] Amran M, Makul N, Fediuk R, Lee YH, Vatin NI, Lee YY, et al. Global carbon recoverability experiences from the cement industry. Case Stud Constr Mater. 2022;17:e01439. doi:10.1016/j.cscm.2022.e01439.
[3] Carvalho IC, Andrade Neto JS, Matos PR, Lothenbach B, Kirchheim AP. The role of foreign ions in Portland cement production and properties: a state-of-the-art review on phase formation, polymorphism and hydration. Cem Concr Compos. 2025;159:105989. doi:10.1016/j.cemconcomp.2025.105989.
[4] Andrade Neto JS, Carvalho IC, Monteiro PJM, de Matos PR, Kirchheim AP. Unveiling the key factors for clinker reactivity and cement performance: a physic-chemical and performance investigation of 40 industrial clinkers. Cem Concr Res. 2025;187:107717. doi:10.1016/j.cemconres.2024.107717.
[5] Zhou Q, Meawad A, Wang W, Noguchi T. Stabilization of metastable calcium carbonate polymorphs on the surface of recycled cement paste particles: a two-step carbonation approach without chemical additives. Cem Concr Compos. 2025;155:105829. doi:10.1016/j.cemconcomp.2024.105829.
[6] Mi R, Rengaraju S, Ai-Tabbaa A. Towards net-zero reinforced concrete: a critical review. Cem Concr Compos. 2025;163(5):106187. doi:10.1016/j.cemconcomp.2025.106187.
[7] Bawab J, El-Dieb A, El-Hassan H, Khatib J. Effect of different activation techniques on the engineering properties of cement-free binder containing volcanic ash and calcium carbide residue. Constr Build Mater. 2023;408:133734. doi:10.1016/j.conbuildmat.2023.133734.
[8] Wang C, Li Y, Wen P, Zeng W, Wang X. A comprehensive review on mechanical properties of green controlled low strength materials. Constr Build Mater. 2023;363:129611. doi:10.1016/j.conbuildmat.2022.129611.
[9] Tran TQ, Kim YS, Dang LC, Do TM. A state-of-the-art review on the utilization of new green binders in the production of controlled low-strength materials. Constr Build Mater. 2023;393(8):132078. doi:10.1016/j.conbuildmat.2023.132078.
[10] Ibrahim M, Rahman MK, Najamuddin SK, Alhelal ZS, Acero CE. A review on utilization of industrial by-products in the production of controlled low strength materials and factors influencing the properties. Constr Build Mater. 2022;325(1):126704. doi:10.1016/j.conbuildmat.2022.126704.
[11] Kumar DR, Kannari LD, Senjuntichai T, Kaewunruen S. Optimization of pond-ash-based controlled low-strength materials with lime and superplasticizer via experiments and supervised machine learning. Results Eng. 2026;29(1):108476. doi:10.1016/j.rineng.2025.108476.
[12] Chen SC, Lin WT, Lin KL, Huang PY. A study on the mixed properties of green controlled low strength cementitious. Mater Sci-Pol. 2021;39(1):59–74. doi:10.2478/msp-2021-0004.
[13] Alinejad A, Sadeghian P, Fam A. Low-carbon gypsum-modified concrete with 80% cement reduction and strength restoration by confinement. J Build Eng. 2025;114:114101. doi:10.1016/j.jobe.2025.114101.
[14] Li J, Ma B, Zhang X, Lu X. Enhancement and mechanism of macro-defect free (MDF) gypsum water resistance achieved by hydrophobic modification. Case Stud Constr Mater. 2024;20(1):e02791. doi:10.1016/j.cscm.2023.e02791.
[15] Zhang L, Mo KH, Tan TH, Hung CC, Yap SP, Ling TC. Influence of calcination and GGBS addition in preparing β-hemihydrate synthetic gypsum from phosphogypsum. Case Stud Constr Mater. 2023;19(4):e02259. doi:10.1016/j.cscm.2023.e02259.

[16] Lin CC, Cheng YH, Hsiao CC. The study on material/air equilibrium partition coefficients and internal diffusion coefficients of volatile organic compounds within recycling green building materials. Constr Build Mater. 2025;490(15):142645. doi:10.1016/j.conbuildmat.2025.142645.
[17] Mittal A, Rakshit D. Utilization of cement rotary kiln waste heat for calcination of phosphogypsum. Therm Sci Eng Prog. 2020;20(2):100729. doi:10.1016/j.tsep.2020.100729.
[18] Zhang Y, Pan F, Wu R. Study on the performance of FGD gypsum-metakaolin-cement composite cementitious system. Constr Build Mater. 2016; 128(2):1–11. doi:10.1016/j.conbuildmat.2016.09.134.
[19] Zhao Q, Da Y, He T, Shi C, Ke Y, Li S, et al. Effect of $Na_2SO_4$ and $Na_2CO_3$ on early performance of non-gypsum/low-gypsum cement: mechanism of synergistic activation with gypsum. Constr Build Mater. 2025;470:140554. doi:10.1016/j.conbuildmat.2025.140554.
[20] Papageorgiou A, Tzouvalas G, Tsimas S. Use of inorganic setting retarders in cement industry. Cem Concr Compos. 2005;27(2):183–9. doi:10.1016/j.cemconcomp.2004.02.005.
[21] Mohammed S, Safiullah O. Optimization of the $SO_3$ content of an Algerian Portland cement: study on the effect of various amounts of gypsum on cement properties. Constr Build Mater. 2018;164(7):362–70. doi:10.1016/j.conbuildmat.2017.12.218.
[22] Lachemi M, Şahmaran M, Hossain KMA, Lotfy A, Shehata M. Properties of controlled low-strength materials incorporating cement kiln dust and slag. Cem Concr Compos. 2010;32(8):623–9. doi:10.1016/j.cemconcomp.2010.07.011.
[23] National Environmental Research Academy (NERA). NIEA R220.20C regulatory standards: test method for marine environmental leaching [Internet]. Taoyuan City, Taiwan: National Environmental Research Academy (NERA); [cited 2026 Jan 1]. Available from: https://www.nera.gov.tw/en-us/Introduction.html.
[24] Ho LS, Jhang BJ, Hwang CL, Huynh TP. Development and characterization of a controlled low-strength material produced using a ternary mixture of Portland cement, fly ash, and waste water treatment sludge. J Clean Prod. 2022;356:131899. doi:10.1016/j.jclepro.2022.131899.
[25] Colman C, Bulteel D, Elkarim BM, Rémond S, Courard L. Expansion of concrete by secondary ettringite formation due to fine recycled aggregates contaminated with gypsum. Adv Cem Res. 2023;35(11):480–8. doi:10.1680/jadcr.22.00043.
[26] Sakai E, Nikaido Y, Itoh T, Daimon M. Ettringite formation and microstructure of rapid hardening cement. Cem Concr Res. 2004;34(9):1669–73. doi:10.1016/j.cemconres.2004.04.021.
[27] El Inaty F, Marchetti M, Quiertant M, Metalssi OO. Effect of curing on the coupled attack of sulfate and chloride ions on low-carbon cementitious materials including slag, fly ash, and metakaolin. Constr Build Mater. 2024;438:137307. doi:10.1016/j.conbuildmat.2024.137307.
[28] Wang F, Du H, Zheng Z, Xu D, Wang Y, Li N, et al. The impact of fly ash on the properties of cementitious materials based on slag-steel slag-gypsum solid waste. Materials. 2024;17(19):4696. doi:10.3390/ma17194696.
[29] Wu Y, Geng J, Zhu H, Jin C, Kang N. Development and characterization of sustainable cement-free controlled low strength material using titanium gypsum and construction waste soil. Materials. 2024;17(23):5698. doi:10.3390/ma17235698.
[30] Gui Y, Zi Z, Shiau J, Yuan S, Hua L, Sun L, et al. Utilizing recycled waste organic muck and phosphogypsum in controlled low-strength materials: an experimental study on engineering properties and environmental safety. Case Stud Constr Mater. 2025;23(8):e05485. doi:10.1016/j.cscm.2025.e05485.
[31] Guo Y, Chen S, Lakhiar MT, Zhuang S, Lakhiar IW. Ternary binders and recycled turbine blade fibres in mortar: reducing embodied carbon in coastal construction. Constr Build Mater. 2025;501:144277. doi:10.1016/j.conbuildmat.2025.144277.
[32] Chen H, Zhang Y, Chen J, Qin Z, Wu P. Effect of fly ash and gypsum on drying shrinkage and mechanical properties of one-part alkali-activated slag mortar. Struct Concr. 2025;26(2):1275–88. doi:10.1002/suco.202400006.
[33] Hanjitsuwan S, Injorhor B, Phoo-ngernkham T, Damrongwiriyanupap N, Li LY, Sukontasukkul P, et al. Drying shrinkage, strength and microstructure of alkali-activated high-calcium fly ash using FGD-gypsum and dolomite as expansive additive. Cem Concr Compos. 2020;114(5):103760. doi:10.1016/j.cemconcomp.2020.103760.
[34] Xue L, Ni Z, Zhou Z, Zhang Z, Xiong H, Wang H, et al. Effects of desulfurized gypsum on shrinkage behavior of alkali-activated slag (AAS) and hybrid alkali-activated cement (HAC). Case Stud Constr Mater. 2025;22:e04320. doi:10.1016/j.cscm.2025.e04320.
[35] Rambe MR, Pohan RF, Patriotika F, Harahap S, Nasution AS. Potential of gypsum waste as a substitution and filler material in concrete manufacturing. Fluida. 2023;16(2):120–31. doi:10.35313/fluida.v16i2.4471.
[36] Claisse P, Ganjian E, Tyrer M. The use of secondary gypsum to make a controlled low strength material. Open Constr Build Technol J. 2008;2(1): 294–305. doi:10.2174/1874836800802010294.
[37] Lu W, Ma B, Su Y, He X, Jin Z, Qi H. Low-energy consumption preparation of fine waterproof cementitious material with high-volume phosphogypsum. J Mater Civ Eng. 2020;32(11):04020329. doi:10.1061/(asce)mt.1943-5533.0003423.
[38] Kopittke PM, Menzies NW, Fulton IM. Gypsum solubility in seawater, and its application to bauxite residue amelioration. Soil Res. 2004;42(8):953–60. doi:10.1071/sr04034.
[39] Othman S. Gypsum and limestone dissolution within fatha formation (middle Miocene) at various pH solutions: a laboratory study. Iraqi Geol J. 2020;53(2B):71–88. doi:10.46717/igj.53.2b.4rs-2020-08-04.
[40] Lin WT, Korniejenko K, Mierzwiński D, Łach M, Cheng A, Lin KL. Feasibility study of waste gypsum as a full replacement for fine aggregates of controlled low-strength material. Mater Proc. 2023;13(1):19. doi:10.3390/materproc2023013019.
[41] Li P, Li W, Yu T, Qu F, Tam VWY. Investigation on early-age hydration, mechanical properties and microstructure of seawater sea sand cement mortar. Constr Build Mater. 2020;249(7):118776. doi:10.1016/j.conbuildmat.2020.118776.
[42] Cai Y, Tao Y, Xuan D, Sun Y, Poon CS. Effect of seawater on the morphology, structure, and properties of synthetic ettringite. Cem Concr Res. 2023;163:107034. doi:10.1016/j.cemconres.2022.107034.
[43] Kapeluszna E, Kotwica Ł, Malata G, Murzyn P, Nocuń-Wczelik W. The effect of highly reactive pozzolanic material on the early hydration of alite–C3A–gypsum synthetic cement systems. Constr Build Mater. 2020;251:118879. doi:10.1016/j.conbuildmat.2020.118879.
[44] Kobayashi M, Takahashi K, Kawabata Y. Deterioration of cement-based materials in low-temperature seawater. Materials. 2023;16(15):5278. doi:10.3390/ma16155278.
[45] Dokduea W, Keawsawasvong S, Tangchirapat W, Jaturapitakkul C. Development of binary and ternary binders made from industrial by-products for producing controlled low-strength materials. J Mater Res Technol. 2025;38(8):4087–99. doi:10.1016/j.jmrt.2025.08.158.
[46] Shin Y, Jang JG, Choi J, Jun G, Park C, Kim GM, et al. Utilization of artificial interior stone sludge as fine aggregate in controlled low-strength material (CLSM). J Build Eng. 2023;71(1):106441. doi:10.1016/j.jobe.2023.106441.
[47] Zhang Z, Zhang Y, Cheng S. Durability of cement-modified phosphogypsum composites under water immersion. In: Proceedings of the 2025 7th International Conference on Civil Engineering, Environment Resources and Energy Materials (CCESEM 2025). Dordrecht, The Netherlands: Atlantis Press International BV; 2025. p. 340–6. doi:10.2991/978-94-6463-902-5_33.
[48] Li G, Zhang J, Niu M, Song Z. The mechanism of alkali-free liquid accelerator on the hydration of cement pastes. Constr Build Mater. 2020;233: 117296. doi:10.1016/j.conbuildmat.2019.117296.
[49] Chen X, Zhang H, Zhou C, Geng Y, Wang YY. Tests and theoretical prediction model for RH evolution in recycled aggregate concrete accounting for the porous physical properties of recycled aggregates. J Mater Civ Eng. 2025;37(4):04025053. doi:10.1061/jmcee7.mteng-19321.
[50] Kaur G, Couperthwaite SJ, Millar GJ. Acid mine drainage treatment using bayer precipitates obtained from seawater neutralization of bayer liquor. Glob Chall. 2018;2(12):1800061. doi:10.1002/gch2.201800061.
[51] Wang S, Zhang W, Jia Z. Solidification/stabilization of waste incineration fly ash by modified calcium aluminate cement. Water Air Soil Pollut. 2024;235(3):163. doi:10.1007/s11270-024-06951-7.
[52] Zhang W, Lang L, Qi Z, Wang YY, Xue Q, Li JS. Muti-scale analysis of solidification/stabilization (S/S) of Pb-contaminated dredged sediment using nano-$SiO_2$ modified cement. J Rock Mech Geotech Eng. 2025;17(9):5781–99. doi:10.1016/j.jrmge.2025.01.010.
[53] Sekhar Das C, Ahmad MR, Zhao XL, Dai JG. Influences of temperatures on the physical and chemical chloride binding of calcium silicate hydrate and Friedel salt at different chloride concentrations. Constr Build Mater. 2025;476(5):141303. doi:10.1016/j.conbuildmat.2025.141303.
[54] Brown P, Bothe J. The system CaO-$Al_2O_3$-$CaCl_2$-$H_2O$ at 23 ± 2°C and the mechanisms of chloride binding in concrete. Cem Concr Res. 2004;34(9):1549–53. doi:10.1016/j.cemconres.2004.03.011.